Metalysis Fray Farthing Chen Process As a Strategic Lunar *In Situ* Resource Utilization Technology

Alex Ellery,[1] Ian Mellor,[2] Priti Wanjara,[3] and Melchiorri Conti[4]*

[1]*Mechanical and Aerospace Engineering Department, Carleton University, Ottawa, Canada.*
[2]*Metalysis Ltd, Rotherham, United Kingdom.*
[3]*National Research Council, Aerospace Structures Materials & Manufacturing, University of Montreal, Montreal, Canada.*
[4]*European Space Research & Technology Centre (ESA-ESTEC), Noordwijk, The Netherlands.*

ABSTRACT

Crucial to permanent occupation of the Moon will be the exploitation of local resources to build a lunar infrastructure. We examine 2 processes—the Metalysis Fray Farthing Chen (FFC) process and metal three-dimensional (3D) printing—as the backbone of a robust and sustainable industrial ecology on the Moon to exploit its raw material resources with husbandry. The Metalysis FFC process is an electrochemical technique that can extract near pure metals from their oxide and silicate forms through cathodic reduction. An anode (graphite) and cathode (metal oxide to be reduced) reside in a bath of molten salt $CaCl_2$ at 900–1,100°C. A voltage is applied and the metal oxide releases oxygen ions into the molten salt, and oxygen is released at the cathode and transferred to the anode as CO or CO_2 gas if the anode is graphite. At the cathode, the metal oxide is reduced into metal plus oxygen through a series of intermediate steps. We outline how the Metalysis FFC process can be leveraged through a handful of chemical preprocessing methods to exploit its versatility. We have demonstrated some preliminary experiments in extracting Ti metal powder from rutile through the Metalysis FFC process, which was subsequently 3D printed into Ti test structures using selective laser sintering. These 2 methods—Metalysis FFC and metal 3D printing—offer unprecedented capabilities for a lunar infrastructure manufacturing chain. In particular, we take note of their high-energy efficiency that will be crucial to lunar in situ resource utilization.

Keywords: sustainable *in situ* resource utilization, Metalysis FFC process, additive manufacturing, lunar industrial ecology, lunar industrialization

INTRODUCTION

Until we transport infrastructure onto the Moon and other extraterrestrial locations that enables the production of useful assets to court all the above, the prospect of human space exploration in any robust sense remains bleak. To construct productive capacity on extraterrestrial locations such as the Moon, we must exploit local resources to drive down the cost of space exploration. Although *in situ* resource utilization (ISRU) is yet to be deployed in support of space missions, it has been actively proposed to reduce the costs of human missions and the principle has recently been demonstrated on Mars.

The European Moon Village is an ambitious concept to build a complete infrastructure of several human-occupied bases on the lunar surface devoted to a range of activities across a diverse set of participants from governments to private interests. This will necessarily require extensive ISRU capabilities to reduce their reliance on Earth-supplied resources.

We review *in-situ* resource utilisation on the Moon as background context to the FFC process (S1). Together, the Metalysis Fray Farthing Chen (FFC) process and metal additive manufacturing offer a sustainable approach to ISRU on the Moon.

***Correction added** on March 10, 2022 after first online publication of January 18, 2022: The surname of co-author Priti Wanjara was misspelled as Wanjari. The byline has been corrected.

 DOI: 10.1089/space.2021.0047

METALYSIS FFC PROCESS

The Metalysis FFC process has widespread applications as a universal chemical processing technique on the Moon. It was originally developed to replace the Kroll process in extracting Ti metal from rutile (TiO_2). In the Kroll process, a series of processes are involved.[1] First, carbochlorination of solid rutile TiO_2 with Cl_2 in a fluidized bed reactor yields $TiCl_4$ liquid at 950°C:

$$TiO_2 + 2Cl_2 + C \rightarrow TiCl_4 + 2CO$$

Ilmenite can be treated similarly directly:

$$2FeTiO_3 + 7Cl_2 + 6C \rightarrow 2TiCl_4 + 2FeCl_3 + 6CO$$

The liquid is evaporated and fractionally distilled for purification. The carbon can be reduced and recycled. Carbochlorination of rutile normally proceeds at 950°C, but lower temperatures at 350–450°C are possible thereby reducing corrosion.[2] Second, reduction of $TiCl_4$ with a more reactive metal such as Mg or Na yields Ti metal sponge and NaCl (or $MgCl_2$) at 500°C:

$$TiCl_4 + 4Na \rightarrow Ti + 4NaCl$$

$$TiCl_4 + 2Mg \rightarrow Ti + 2MgCl_2$$

Electrolysis of $MgCl_2$ or NaCl recycles Mg and Na. By contrast, the Metalysis FFC process extracts Ti metal from rutile more efficiently than the Kroll process producing 1 kg Ti from 1.66 kg rutile.[3] It is an electrochemical technique that reduces powdered oxide at the cathode into high-purity metals (>99% pure). The raw mineral oxide requires physical preprocessing through powdering, compacting, and sintering into a cathode rod. It is inserted into an electrolytic cell with the molten alkaline earth salt $CaCl_2$ as the electrolyte at around 900°C in conjunction with an appropriate anode.[4] $CaCl_2$ electrolyte melts at 762°C and dissolves its own oxide (CaO) at 900°C even at low voltages over 2.5 V, but 3 V is adopted nominally for the electrolytic voltage.[5]

The metal oxide is in sintered powder form acting as the cathode despite being nonconducting and is directly reduced to metal in the solid state. Due to the brittleness of metal oxides, they can be ground to a finer powder than the metal form thereby offering finer grained metal powder after processing. Multiple oxides may be treated simultaneously at different cathodes to create different metals in the same cell. The required heating to 850–1,100°C is modest, but electrolytic energy is required to split all the mineral components. The cathode is reduced to sintered solid pure metal sponge releasing O^{2-} ions into the electrolyte solution, which are transported to the graphite anode to form CO/CO_2 gas, which is released:

$$\text{Cathode}: MO_x(s) + 2xe^- \rightarrow M + xO^{2-}$$

$$\text{Anode}: C + O^{2-} \rightarrow CO + 2e^- \text{ and } C + 2O^{2-} \rightarrow CO_2 + 4e^-$$

Nominally, a graphite anode is used and consumed through oxidation yielding anode-evolved CO/CO_2 gas. Any metal oxide can be reduced in this manner—essentially, this is an electrolytic version of carbothermal reduction of mineral oxides. Reduction of the metal oxide occurs in the solid state without melting, yielding lower energy consumption. The $CaCl_2$ electrolyte is not consumed (except through retention of electrolyte by porous cathodes) and is recycled, requiring only Cl imported from the Earth to replenish the small losses in porous cathodes. In a lunar context, the addition of CaO derived from anorthite to the electrolyte enhances electrolytic conductivity to a current of 4 A while the electrolytic cell may be contained in an alumina crucible.

The graphite anode is consumed and must be replaced. To obviate against the loss of graphite anodes, an inert anode would be desirable to release O_2 gas directly ($2O^{2-} \rightarrow O_2 + 4e^-$). SnO_2 doped with 2% Sb_2O_3 and 1% CuO was successful as an inert anode, but it eroded rapidly due to the formation of $CaSnO_3$; a more promising anode was a solid solution of calcium titanate and calcium ruthenate ($CaTi_xRu_{1-x}O_3$), which offered negligible degradation.[6] An inert anode may be constructed from ferrites or cermet (nickel/ferrite mixture), which could be sourced on the Moon, but this is yet to be explored.

Other potential anode materials include NiO, $CaTiO_3$, or $Ca_2Fe_2O_5$ (subject to existing patents filed in 2006), which are also derivable from lunar resources. Graphite anodes are well established, but capturing and recycling the CO/CO_2 gas and reducing it to carbon will be necessary to conserve the carbon. CO/CO_2 may be recycled through the Sabatier reaction—this is an example of a potential lunar field test of ISRU techniques required for human Mars missions. First, the CO component may be fully burned, but this may be performed at low temperature in the presence of a spinel catalyst at 30–350°C[7]:

$$CO + 0.5\,O_2 \rightarrow CO_2$$

The Sabatier reaction with hydrogen occurs at 300°C reconstituting methane:

$$CO_2 + 4H_2 \rightarrow CH_4 + 2H_2O$$

If required, the water can be electrolyzed to recover oxygen and the hydrogen recycled. Methane may be pyrolytically split into carbon and hydrogen at 1,400°C using an Ni catalyst:

$$CH_4 \rightarrow C + 2H_2$$

This would regenerate the carbon required for the graphite anode. Other options include reduction of CO through the Boudouard reaction at 700°C:

$$2CO \rightarrow C + CO_2$$

Further reduction is achieved through the Bosch reaction at 530–730°C with an Fe catalyst:

$$CO_2 + 2H_2 \rightarrow C + 2H_2O$$

Heating of the electrolyte to the modest 900°C could be accomplished through solar concentrators such as Fresnel lenses. We have demonstrated Fresnel lens smelting of Zn-Al alloy (Zn additive prevents oxidation, which is unnecessary under the vacuum conditions on the Moon) at 800°C using a 1.2 m × 0.9 m lens with a focal length of 1 m under field conditions (*Fig. 1*).

The maximum temperature T achievable by a solar concentrator is given by[8]:

$$T = \left(\frac{CS_0}{\sigma}\right)^{1/4}$$

where $C = \frac{A_r}{A_a} = \frac{n^2}{sin^2\theta}$ = concentration ratio (ratio of radiating-to-absorber area) = 2,000 being readily achievable,[9] σ = Stefan/Boltzmann constant, S_0 = solar radiation density = 1,358 W/m^2 for the Moon, θ = incident radiation acceptance half angle, and n = refractive index of transparent covering on absorber. Sintering requires heat fluxes of 50 W/cm^2 to generate regolith temperatures of 1,000°C. A set of solar parabolic mirror concentrators of 1.5 m^2 area may be focused to melt lunar regolith at ~1,600°C. For C_a = 1,000 (such as a scaled-up 3 m lens focused on a 5-cm-diameter furnace spot), T_{max} > 2,000 K, which is more than sufficient to melt or vaporize common metals and silica/quartz.

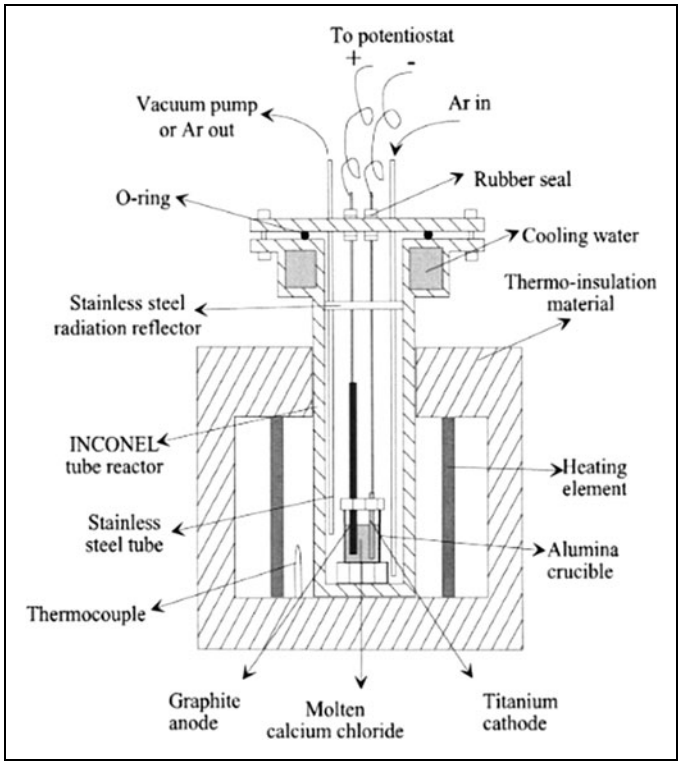

Fig. 1. Metalysis FFC process cell. FFC, Fray Farthing Chen.

A larger solar furnace can generate temperatures of 2,200–2,700°C to potentially vaporize lunar regolith, but this is unnecessary in this context. However, increased pressure within reaction vessels can also reduce crucible temperatures required for Fresnel lens as thermal transmission may be conveyed through quartz rods into the reactor vessel.

The distribution of thermal energy through the electrolytic bath may prove challenging. A stirring mechanism must be implemented to distribute heat flux through the electrolyte—the low gravity permits exploitation of buoyancy-driven thermal convection. Alternatively, the use of high-temperature silica optical fibers can transfer concentrated solar radiation and distribute thermal energy through the bath. An array of solar parabolic concentrators has demonstrated the transfer of solar energy through a secondary optical funnel to an optical waveguide constructed from optical fibers to provide more uniform heating.[10] It delivered up to 1,000 W/m^2 to regolith to generate 1,800°C sufficient for carbothermal reduction with an overall efficiency of >40%.

Electrical energy may be supplied through thermionic conversion with losses in conversion efficiency, but the electrical energy requirement of around 3% is dwarfed by the thermal energy requirement of the furnace of ~97% (*Table 1*). It cannot be emphasized enough how important this factor is in relation to lunar ISRU because significant amounts of energy loss are encountered in the conversion of light/thermal energy into electrical energy. Since 97% of the energy input to the Metalysis FFC process is thermal, with only 3% electrical, this ensures maximum energy efficiency with minimal energy losses.

Table 1. Power Requirements for the Metalysis Fray Farthing Chen Cambridge Process for Generation 1 Cell and the Scaled-Up Generation 2 Cell

Generation 1		*Generation 2*	
Furnace	5 kW	Furnace	60 kW
Salt volume	0.001 m^3	Salt volume	0.25 m^3
Electrolysis power	175 W	Electrolysis power	1,750 W
Postprocessing power	0.1 kW	Postprocessing power	100 kW

The solar concentrators may be used in conjunction with vacuum tube-based thermionic conversion to generate electrical energy.[11] Efficiencies of 20% are typical of the Russian nuclear reactor thermionic conversion with $T_C = 1{,}650°C$ at the cathode and $T_A = 650°C$ at the anode.[12] Thermionic conversion requires vacuum tube materials—glass, tungsten, nickel, and kovar, which can be sourced on the Moon.

There are a number of potential improvements to thermionic conversion efficiency. The use of electric potential shaping can increase efficiencies up to 40%.[13] A second thermoelectric conversion stage (*e.g.,* Mg_2Si) may yield up to 30% efficiencies.[14] Photon-enhanced thermionic conversion[15,16] adds a photovoltaic stage for up to 50% efficiencies that may be implemented with aluminum-doped hematite photocathodic coatings[17] (formed from ilmenite-derived iron heated in oxygen) or other photoconductive coatings. *In situ* thermionic conversion approaches offer greater efficiencies than *in situ* resourced solar cells.[18,19]

However, it may conservatively be estimated that thermionic-electrical conversion efficiencies are unlikely to exceed 30% in a lunar context from *in situ* manufactured thermionic converters. Hence, the Metalysis FFC process can be implemented through solar thermal energy with only a small supplement of electrical energy to minimize energy conversion losses compared with full electrical energy supply (as adopted on the Earth).

DIRECT APPLICATION OF METALYSIS FFC PROCESSING TO LUNAR RESOURCES

In its most obvious application, the Metalysis FFC process can be applied directly to lunar minerals without preprocessing to yield mongrel alloys. Whereas commonly used alloys typically comprise a single dominant metal with the addition of small amounts of other metals, mongrel alloys are dependent on the initial constituents of the mineral, which almost certainly do not correlate with desirable alloys. Most experiments performed with the lunar regolith simulant will not replicate lunar regolith actual in this context—they are constructed from terrestrial constituents that approximate most of the physical, but only some of the chemical, properties of lunar regolith. Many of the subtle and minor constituents will not be represented accurately.

Most of these experiments are concerned with the extraction of oxygen rather than the metal residue, and so, the fidelity of simulants is of reduced concern. In our context, however, this aspect will be crucial and is currently unexplored. The Metalysis FFC process at 900°C has been applied to a sintered pressed solid lunar regolith simulant (JSC-1 representing mare regolith) in a molten $CaCl_2$ electrolyte with an applied potential of 3V.[20] A powder bed of loose regolith simulant (30 g) rather than a powder bed of pressed and sintered powder has yielded a 96% (4.5 g) oxygen recovery rate after 50 h of operation.[21]

The metallic products of metal alloy were enriched in Al/Fe, Fe/Si/Al, and Ca/Al/Si/Mg, suggesting a degree of metal specificity. However, it is unclear how discriminatory this specificity is, and indeed, how representative this is to the lunar regolith constituents. In the case of lunar minerals, we expect the resultant mongrel alloys following reduction (ignoring minor constituents) to involve:

1. extraction of FeTi amalgam and O_2 from lunar ilmenite ($FeTiO_3$);
2. extraction of Al-Si-Ca alloy and O_2 from lunar anorthite ($CaAl_2Si_2O_8$); and
3. extraction of MgSi alloy and O_2 from lunar olivine (Mg_2SiO_4).

We have not examined pyroxene reduction as pyroxene has highly variable constitutions of the form $(Ca,Mg,Fe)_2Si_2O_6$, but see *Table 2* for the use of pyroxene with HCl treatment.

The Metalysis FFC process can reduce ilmenite ($FeTiO_3$) yielding TiFe and $TiFe_2$ alloy sponge, which may be crushed into a metal powder—experiments with a sintered ilmenite powder cathode yielded 90% oxygen recovery (32 kg) from rutile mineral (100 kg).[22] The general FeTi alloy may be used for general purpose structures; ferrotitanium alloy (45%–75% Ti) may be used as an oxygen getter or as a pyrotechnic powder fuel with an O_2 oxidant. Its oxygen-scavenging properties do not prevent its general use on the Moon, but it should not be used where free O_2 is in proximity (such as habitat interiors).

The Metalysis FFC process may reduce lunar olivine (Mg_2SiO_4) directly into MgSi alloy. MgSi alloys may be used for general purpose structures—small amounts of Mg_2Si alloy are added to Al to produce high-strength Al alloy and can tolerate small proportions of Fe contamination characteristic of lunar olivines of Fe:Mg ratios of ~1:4 to 2.3.[23] The 6061 series is the commonest aluminum alloy and has minor additives of 0.8%–1.2% Mg, 0.4%–0.8% Si, 0%–0.7% Fe, and 0%–0.25% Ti (Cr and Mn may be omitted as they impart oxidative corrosion resistance). Mg_2Si is also a thermoelectric material but with poor efficiency.

The Metalysis FFC process may also reduce the $MgAl_2O_4$ spinel to MgAl alloy (such as magnalium used as a lightweight corrosion-resistant alloy or solid fuel if ground into powder), but this would require that it be separated out from the other products of Mg, AlSi alloy, and pure Si.

The Metalysis FFC process can reduce lunar anorthite ($CaAl_2Si_2O_8$) from highland regions to AlCaSi alloy—a

Table 2. Near Closed-Loop Lunar Industrial Ecology (Emboldened Materials Are Pure Metal Oxides for Direct Reduction Using the Metalysis Fray Farthing Chen Process)

Lunar Ilmenite

$Fe^0 + H_2O \rightarrow$ ferrofluidic sealing

$FeTiO_3 + H_2 \rightarrow \mathbf{TiO_2} + H_2O + Fe$

$2H_2O \rightarrow 2H_2+O_2$

$2Fe + 1.5O_2 \rightarrow Fe_2O_3/Fe_2O_3.CoO$ - ferrite magnets

$3Fe_2O_3 + H_2 \leftrightarrow Fe_3O_4 + H_2O$) – formation of magnetite at 350-750°C/1-2 kbar

$4Fe_2O_3 + Fe \leftrightarrow 3Fe_3O_4$)

Nickel-Iron Meteorites

W inclusions → Thermionic cathodic material

Mond process:

		Alloy	Ni	Co	Si	C	W
$Fe(CO)_5 \leftrightarrow 5CO + Fe$ (175°C/100 bar)	→	Tool steel				2%	9-18%
$Ni(CO)_4 \leftrightarrow 4CO + Ni$ (55°C/1 bar)	→	Electrical steel			3%		
$Co_2(CO)_8 \leftrightarrow 8CO + 2Co$ (150°C/35 bar)	→	Permalloy	80%				
$W(CO)_6 \leftrightarrow 6CO + W$		Kovar	29%	17%	0.2%	0.01%	

S catalyst

$4FeS + 7O_2 \rightarrow \mathbf{2Fe_2O_3} + 4SO_2$

(Troilite) $SO_2 + H_2S \rightarrow 3S + H_2O$

$FeSe + Na_2CO_3 + 1.5O_2 \rightarrow \mathbf{FeO} + Na_2SeO_3 + CO_2$

KNO_3 catalyst $Na_2SeO_3 + H_2SO_4 \rightarrow Na_2O + H_2SO_4 + Se \rightarrow$ photosensitive Se

↑_____|

$Na_2O + H_2O \rightarrow 2NaOH$

$NaOH + HCl \rightarrow NaCl + H_2O$

Lunar Orthoclase

$3KAlSi_3O_8 + 2HCl + 12H_2O \rightarrow KAl_3Si_3O_{10}(OH)_2 + 6H_4SiO_4 + 2KCl$

orthoclase illite silicic acid (soluble silica)

$2KAl_3Si_3O_{10}(OH)_2 + 2HCl + 3H_2O \rightarrow 3Al_2Si_2O_5(OH)_4 + 2KCl$

kaolinite

$[2KAlSi_3O_8 + 2HCl + 2H_2O \rightarrow Al_2Si_2O_5(OH)_4 + 2KCl + \mathbf{SiO_2} + H_2O]$

$KCl + NaNO_3 \rightarrow NaCl + KNO_3$

Lunar Anorthite

$CaAl_2SiO_8 + 2HCl + H_2O \rightarrow Al_2Si_2O_5(OH)_4 + CaCl_2$ → FFC electrolyte

Kaolinite 100°C

$Al_2Si_2O_5(OH)_4 + 6HCl \rightarrow 2AlCl_3 + 2\mathbf{SiO_2} + 5H_2O$ → fused silica glass

400°C

$2AlCl_3.6H_2O \rightarrow \mathbf{Al_2O_3} + 6HCl + 9H_2O \rightarrow 2Al + Fe_2O_3 \rightarrow 2Fe + Al_2O_3$ (thermite)

↑_____| → AlNiCo hard magnets

→ Al solar sail

$CaAl_2SiO_8 + 4C \rightarrow CO + \mathbf{CaO} + \mathbf{Al_2O_3} + 2Si$ at 1650°C → CaO cathode coatings

$CaO + H_2O \rightarrow Ca(OH)_2$

$Ca(OH)_2 + CO_2 \rightarrow CaCO_3 + H_2O$

Lunar Pyroxene

$Ca(Fe,Al)Si_2O_6 + HCl + H_2O \rightarrow Ca_{0.33}(Al)_2(Si_4O_{10})(OH)_2.nH_2O + H_4SiO_4 + CaCl_2 + Fe(OH)_3$

Augite montmorillonite silicic acid iron hydroxide

Lunar Volatiles

850°C 250°C

$CH_4 + H_2O \rightarrow CO + 3H_2 \rightarrow CH_3OH$ 350°C

Ni catalyst Al_2O_3 $CH_3OH + HCl \rightarrow CH_3Cl + H_2O$ 370°C +nH_2O

Al_2O_3 $CH_3Cl + Si \rightarrow (CH_3)_2SiCl_2 \rightarrow ((CH_3)_2SiO)_n + 2nHCl$ → silicone plastics/oils

↑_____|

$N_2 + 3H_2 \rightarrow 2NH_3$ (Haber-Bosch process)

Fe on $CaO+SiO_2+Al_2O_3$

$4NH_3 + 5O_2 \rightarrow 4NO + 6H_2O$

WC on Ni

$3NO + H_2O \rightarrow 2HNO_3 + NO$ (Ostwald process)

↑_____|

$2SO_2 + O_2 \leftrightarrow 2SO_3$ (low temp)

$SO_3 + H_2O \rightarrow H_2SO_4$

Salt of the Earth

$2NaCl + CaCO_3 \leftrightarrow Na_2CO_3 + CaCl_2$ (Solvay process) → FFC electrolyte

350°C/150 MPa

$Na_2CO_3 + SiO_2(i) \leftrightarrow Na_2SiO_3 + CO_2$ → piezoelectric quartz crystal growth (40-80 days)

1000-1100°C

$CaCO_3 \rightarrow \mathbf{CaO} + CO_2$ (calcination)

$NaCl(s) + HNO_3(g) \rightarrow HCl(g) + NaNO_3(s)$

Metalysis FFC Process ($CaCl_2$ electrolyte)

$MO_x + xCa \rightarrow M + xCaO \rightarrow M + xCa + ½xO_2$ where M=Fe, Ti, Al, Mg, Si, etc

$CO + 0.5\ O_2 \rightarrow CO_2$

$CO_2 + 4H_2 \rightarrow CH_4 + 2H_2O$ at 300°C (Sabatier reaction) → $CH_4 \rightarrow C + 2H_2$ at 1400°C for FFC anode regeneration

Ni catalyst

Earth-imported NaCl is used as a source of recycled reagents, and so, is not consumed. Lunar volatiles that are similar are used as recycled reagents and are not consumed. The exception is carbon volatiles that may be used to manufacture silicone plastic elastomers, but if electrical insulation is implemented with glass cloth, the requirement for silicones will be minimal.

sintered cathode of anorthite may be reduced to yield Al, Ca, and Si alloy. AlCaSi alloy may be used for general purpose structures. If Ca can be removed, aluminum/silicon is a common filler metal used for brazing aluminum. Brazing involves melting a lower melting point filler to join 2 metal parts in a gas flux to prevent oxidation (unnecessary in a vacuum).

Nickel alloy is used for joining steels, while cobalt is used for joining superalloys, but brazing does not have the high strength of a welded joint. AlSi alloys (20%–50% Si) are used for welds, through which the Si provides fluidity with low shrinkage. As they solidify, the Si particles provide high wear resistance and low thermal expansion. To compensate for Fe contamination, Ni and Co may be added to improve strength (which may be sourced from *in situ* NiFe meteorite material).

AlSi alloy exhibits lower viscosity than pure aluminum and is suitable for casting or powder metallurgy. Etching yields a hardened, highly wear-resistant silicon precipitate that is porous enough to retain oil that is suitable for linerless reciprocating components. Silumin (3%–25% Si) alloy is an AlSi alloy used for high durability applications such as in the lining of moving parts for machines such as pistons. However, it is likely that these specialist metal alloys will require extensive preprocessing to yield the required proportions for the desired properties.

The properties of these mongrel alloys (and indeed, those resulting from pyroxene reduction)—FeTi, AlCaSi, and MgSi—need to be investigated further. There are certainly some potential uses, including structural uses. The specialized applications of the mongrel alloys are insufficiently useful to justify the use of the Metalysis FFC process directly to unprocessed lunar minerals—most of the utility of the alloys requires extensive preprocessing to remove specific components from the melt, for example, silumin requires the removal of Ca. It is an open question whether structural uses of mongrel alloys are competitive with alternatives.

Compressive structures may be constructed on the Moon using raw regolith—JSC-1AC lunar regolith simulant, comprising dominantly plagioclase with some olivine and pyroxene, has been processed using a 2 J/mm^2 laser energy to melt the regolith and form dense amorphous structures through thermal three-dimensional (3D) printing.[24] As we shall see, single-species metals can be extracted if chemically preprocessed, affording highly tailorable functional properties in alloy design.

CHEMICAL PREPROCESSING OF LUNAR RESOURCES FOR THE METALYSIS FFC PROCESS

The versatility of the Metalysis FFC process is best realized in the reduction of pure metal oxides into pure metals with well-defined functional properties, which can also be mixed into precisely constituted alloys with tailored functional properties. Hence, we must use thermochemical preprocessing to reduce mixed metal lunar minerals into pure elemental metals, from which desired alloys can be constructed. On Earth, most ores are oxides (*e.g.,* bauxite, hematite, and rutile) although some are sulfides (*e.g.,* pyrite and chalcopyrite). Typically, metal sulfides are preprocessed by roasting in air into metal oxides and sulfur dioxide and then processed as metal oxides, that is, preprocessing is well established.

Although ores do not exist on the Moon, lunar minerals—primarily silicates—must similarly be thermally processed into pure metal oxides. A simple example of this shown earlier is ilmenite being reduced pyrochemically to recover Fe and O_2 and the resultant rutile (TiO_2), which may be reduced in molten $CaCl_2$ electrolyte through the Metalysis FFC process to Ti metal while extracting over 99% of the oxide component. Ulvospinel can also be reduced in a similar manner to yield rutile, iron, and oxygen, with the rutile reduced to Ti metal using the Metalysis FFC process. Rutile (TiO_2) in powdered form (*Fig. 2a*) was the feedstock to the Metalysis FFC process and was reduced directly to Ti metal powder (*Fig. 2b*). Some residual impurities, including iron, may be useful in producing titanium alloys.

We may use other preprocessing approaches to other lunar minerals to render single-metal oxides. Most simply, we can use some pure metals and mongrel alloys for reduction. Magnesian olivine (forsterite) may be subjected to aluminothermic reduction in the appropriate proportions at 1,000°C:

$$3Mg_2SiO_4 + 6Al \rightarrow 2MgAl_2O_4 + 4MgO + 2AlSi + Si$$

MgO can be reduced using the Metalysis FFC process or, alternatively, MgO can be reduced by AlSi by continuing the reaction at 1,000°C to yield Mg metal:

$$4MgO + 2AlSi \rightarrow MgAl_2O_4 + 3Mg + 2Si$$

Molten Mg above 650°C enables it to be tapped from the refractory oxide and Si metal sponge. Magnesium is used in the production of magnesium alloy—since it is primarily alloyed with aluminum, reduction of $MgAl_2O_4$ using the Metalysis FFC process produces an alloy excessively rich in Al (most magnesium alloys include 3%–13% aluminum and traces of Mn). The case for magnesium alloy over aluminum *per se* is marginal for general purpose structural applications.

However, Magnox is a highly specialized magnesium alloy (Mg plus 0.8% Al and 0.004% Be) used for cladding fissile material up to 415°C, but the omission of Be eliminates its

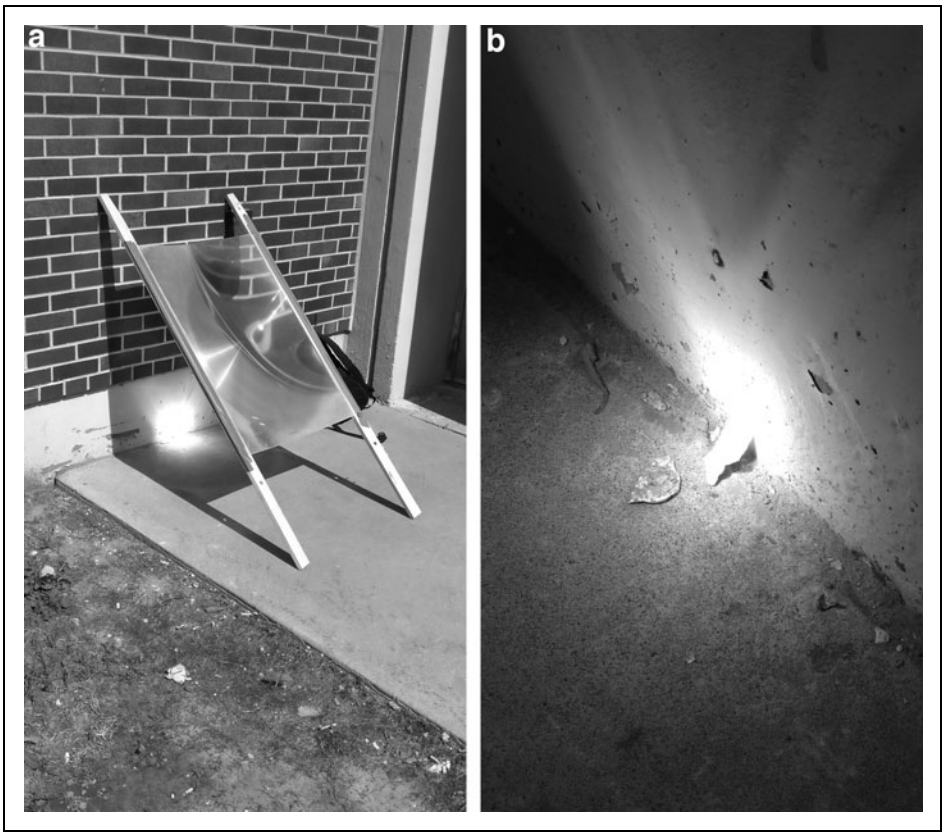

Fig. 2. Smelting of Al alloy pieces using a Fresnel lens-based solar concentrator.

most desirable properties of low-neutron capture cross section. Magnetite (ferrite) may be manufactured from ferric olivine (fayalite) from chondritic sources on the Moon through oxidation at 400–700°C:

$$6Fe_2SiO_4 + 2O_2 \rightarrow 3Fe_3(SiO_4)_2 + Fe_3O_4$$

The product magnetite may be used to form ferrites, including cobalt ferrite used as a hard magnetic material in electric motors.

If anorthite is processed beforehand, Al and Si metals may be extracted as elemental metals. Ca and Si are desirable although the former might not be as valuable as Al (although Ca is a better conductor than Cu or Al, but its specific conductivity is inferior to Al). Aluminum is versatile as a structural material as it is lighter and easier to machine than steel and as electrical/thermal conducting wire, and it is used instead of copper for overhead electricity cabling with two-thirds of its electrical conductivity. Aluminum is typically used for high-reflectivity mirrors and its light weight favors its use in solar sails as thin films.

Alnico (8%–12% Al, 15%–26% Ni, 5%–24% Co alloy with minor amounts up to 6% Cu and up to 1% Ti, the rest being Fe) offers high-coercivity (permanent) magnetism intermediate between iron-based and rare Earth-based magnets for electric motors with a high-temperature tolerance up to 530°C (higher than rare earth magnets). Different combinations offer different properties (such as brittleness and corrosion resistance), and so, it is unclear what effect the omission of Cu will have. Aluminum powder mixed with iron oxide powder when ignited undergoes a rapid thermite reaction that is used for welding metal (historically, for welding railway tracks). Hence, aluminum has a wide versatility of functions. There are several options for processing anorthite as a source of aluminum.

We propose an artificial weathering approach (using hot concentrated HCl rather than dilute carbonic acid H_2CO_3) yielding silica, clays, and other nontoxic products (see our lunar industrial ecology of *Table 2*). If HCl is imported from Earth (in NaCl form for *in situ* conversion into HCl), acid leaching by HCl is a viable approach to reducing anorthite via kaolinite while avoiding high temperatures requiring only modest heating to accelerate the reaction[25]:

$$CaAl_2Si_2O_8 + 8HCl + 2H_2O \rightarrow CaCl_2 + 2AlCl_3.6H_2O + 2SiO_2$$

The advantage of the artificial weathering approach is that it also produces $CaCl_2$ electrolyte as a by-product to replenish potential losses of the Metalysis FFC electrolyte—it represents a lunar analogue to the terrestrial recycling of $CaCl_2$ as a waste product of the Solvay process. Aluminum chloride hexahydrate ($AlCl_3.6H_2O$) may be melted above 100°C to separate it from $CaCl_2$ and SiO_2—it may subsequently be heated to yield alumina at 400°C:

$$2AlCl_3.6H_2O \rightarrow Al_2O_3 + 6HCl + 3H_2O$$

Alumina may be subjected to the Metalysis FFC process to yield Al metal as a lunar analogue to the Hall/Heroult process.

One of the products of artificial weathering is silica, which is rare on the Moon, which may be precipitated out from silicic acid solution. Silica may be used as a ceramic (such as in fiber or wool form), for fused silica glass manufacture for high-grade optical components, and/or reduced to silicon metal (primarily as an alloy additive). Lunar aluminosilicate such as

anorthite may be adopted as the basis for glass on the Moon—aluminosilicate (57% SiO_2, 20% Al_2O_3, 12% MgO, 5% CaO) glasses have a melt temperature of ~1,100–1,350°C, which is significantly lower than the 1,700°C required of fused silica.[26] However, the moderate to high FeO content causes glass darkening, which is undesirable for transparency, and so, it would have to be removed, but this will be difficult.

Aluminosilicate glass may be used in fiber form for glass fabric or wool for electrical and/or thermal insulation or for structural reinforcement in aluminum metal, for example, ceramic composites such as Al_2O_3 particles/fibers have been embedded in an Al metal matrix to yield high-strength materials.[27] However, for transparent optical components, fused silica glass eliminates the problem of iron darkening in natural glasses. High-purity silica may be accomplished by heating SiO_2 in an H_2-O_2 flame in the presence of $SiCl_4$ vapor:

$$SiCl_4 + 2H_2 + O_2 \rightarrow SiO_2 + 4HCl$$

SiO_2 may be reduced to silicon metal by the Metalysis FFC process at 850°C, with multiple metal wire electrode contact points in the bulk material supplying electrons.[28] It yields metallurgical purity requiring it to be further purified for use in solar photovoltaics/electronics. Powdered Si metal may be reacted with HCl at 300°C yielding the volatile trichlorosilane liquid:

$$Si + 3HCl \rightarrow HCl_3Si + H_2$$

Removal of H_2 allows reversal to yield purified polysilicon:

$$HCl_3Si \rightarrow Si + HCl + Cl_2$$

Purification of Si permits recycling of chlorine. The degree of purification achievable under lunar conditions is unclear and the purity requirements for electronics are extremely stringent. Apart from enstatite ($MgSiO_3$), one of the few uses of pyroxenes due to their nature as complex solid solutions of metal silicates is as a source of silica on treatment with HCl acid.

HCl can be manufactured *in situ* from NaCl salt rather than importing it as an acid. A similar notion proposed leveraging of aluminum, silicon, glass, and oxygen from lunar resources by the import of KF from Earth, which may be salt electrolyzed into K and F,[26] but fluorine-based reactions are aggressive. A similar artificial weathering method may be applied to lunar orthoclase to release K salts as reagents (in the lunar industrial ecology of *Table 2*). A second process that may be applied to anorthite is carbothermal reduction to alumina feedstock directly at 1,650°C:

$$CaAl_2Si_2O_8 + 4C \rightarrow CaO + Al_2O_3 + 2Si + 4CO$$

The mixture of metal oxides and silicon requires separation after powdering. The addition of Al metal powder at high temperature scavenges oxygen (by forming Al_2O_3) and reduces CaO to Ca metal under vacuum conditions, which may be tapped off as liquid above 842°C. However, contamination is certain, and liquid aluminum absorbs calcium to form AlCa alloy making the extraction of pure Ca inviable.[29] Nevertheless, CaO without reduction has utility as a low work function coating for thermionic cathodes. The advantage of ready CaO recovery with direct Al_2O_3 and Si manufacture through carbothermic reduction of anorthite must be traded against its high temperature. We have included both methods in our lunar industrial ecology (*Table 2*).

Unlike most electrolytic techniques that are highly material specific and bespoke, the Metalysis FFC process can be applied to many metal oxides to yield high-purity metals for future generations of ISRU evolutions offering an unrivaled one-process-fits-all technique. It exhibits low-energy consumption due to the low temperatures required because the oxides or metals do not require melting. Metal oxides may be presented in a mixed prealloy form to combine metals that cannot otherwise be combined due to disparate melting points. The solid-state operation permits the creation of alloys that combine low melting point and high melting point metals where the melting temperature of one (such as W) is greater than the boiling temperature of the other (such as Al).[30]

Mixed oxides can thus be processed regardless of melting points to form unique alloys, including metal alloys from mixed oxide powders such as titanium aluminide TiAl, which has excellent high-temperature properties from TiO_2 and Al_2O_3 reactants.[31] The manufacture of the shape memory alloy NiTi alloy from Ni and Ti oxides introduces the possibility for artificial muscle actuators from lunar resources.[32] The shape memory effect involves a transformation between a low-temperature martensite crystalline phase and a high-temperature austenite crystalline phase. If deformed in the martensite phase followed by heating above a critical temperature, the reverse transformation can be induced. Superelasticity is another property of the shape memory effect.

If drawn to thin diameters <200 μm thick, NiTi can yield 100% strains. In their superelastic phase, NiTi exhibits a similar stress/strain characteristic of a human tendon. NiTi wires are made through casting using vacuum arc or induction melting and drawing into wire. Training occurs with shaping at 400–500°C for 30 min, then quenched. Shape memory materials may be embedded in structures where their electrical resistance generates self-heating for vibration-suppression. They may also be adopted as sheets for controlling solar sails.[33] Future possibilities for the Metalysis FFC process with

more extensive material recovery from potassium-rare earth elements-phosphorus minerals include permanent magnetic NdFeB and superconducting NbTi alloys.

It is apparent that in conjunction with preprocessing schemes, the Metalysis FFC process promises a wide variety of metals from lunar minerals. Indeed, it forms the linchpin of our lunar industrial ecology that incorporates preprocessing within a framework of recycling to ensure that all reagents are recycled and reconstituted (*Table 2*). We have discussed only a subset of the lunar industrial ecology, but present the entire architecture for completeness.

ADDITIVE MANUFACTURING OF METALS

A common approach to the execution of multiple manufacturing tasks is to develop specialized optimized machinery to achieve each individual task. These manufacturing methods are typically subtractive, for example, casting, milling, turning, and forging, which require specialized tooling and invoke a significant waste of material (swarf and tailings). This is not an option for planetary ISRU where resources must be husbanded and tasks may be unanticipated and require adaptability.

3D printing or additive manufacturing is a highly versatile mode of manufacture that lends itself to adaptability.[34] It has been applied to the construction of structures from regolith stimulants.[35] 3D printing permits the manufacture of structural designs that cannot be manufactured through subtractive techniques—it can construct complex shapes with complex internal geometries without specialized tooling. Component parts may be merged into complex monolithic structures, reducing the requirement for assembly joints and assembly tasks.

The implementation of 3D printing provides for the monolithic construction of secondary structure such as support brackets and even mechanical joints integrated with primary structures. It is a tool-less manufacturing technique that minimizes waste through its additive property and recycling of feedstock. 3D structures are built up sequentially layer-by-layer directly from a sliced CAD model. Layer thickness resolution and density are determined by powder particle size and additive processing parameters—metal powders of optimal particle size $\sim$20–150 μm yield similar layer thicknesses of 20–100 μm.

It is reckoned that subtractive methods require 10 times as much material as that encapsulated in the final product—additive manufacturing almost eliminates this entirely and thus affords a significant advantage for ISRU where waste is expensive in both material and energy.

The application of additive manufacturing to space and/or planetary environments is challenging as well as offering advantages: (1) lack of atmosphere makes metal powder vacuum weld into clumps; (2) metal and ceramic powders are considered a potential health hazard, but it is likely that ambient lunar dust constitutes a greater threat; (3) ambient vacuum of the Moon prevents oxidation during sintering/melting; (4) powder deposition is not conducive to microgravity environments, but this condition is relaxed in low-gravity environments; (5) low gravity may result in delamination between layers; and (6) low gravity reduces support structure requirements.

The concern over the use of powder is moot in the context of robotic factory facilities on the Moon as there is an ambient gravity field (assistable by vibration) and there is no human particulate infection issue in an automated factory environment.

The output of the Metalysis FFC process is metal alloy powder that may serve as feedstock for powder metallurgy and powder bed metal 3D printing. This bypasses the usual step required for powder production through atomization of molten metal by water jets. The high cooling rates yield particles of $\sim$1–500 μm of irregular shapes typically contaminated with oxides. Gas atomization by an inert gas such as nitrogen or argon is superior yielding spherical particles with an average particle size of 40 μm. Although smaller particle sizes favor a smoother surface finish, <20-μm-sized particles introduce flowability problems in the powder.

Nevertheless, the Metalysis FFC process forgoes this step by powdering and sintering its original brittle oxide form using traditional ball milling, which as ceramic particles, unlike metal powders, are not subject to vacuum welding. After reduction to metal, the resultant metal is easily powdered and then subjected to a wide range of 3D printing techniques.

The metallurgy of 3D-printed metal parts is essentially similar to that of parts manufactured traditionally, but often with superior physical properties such as hardness. Metal additive manufacturing yields fully dense metal parts through the omission of binders. The 2 commonly adopted metal 3D printing platforms are as follows: (a) powder bed fusion (PBF) and (b) direct energy deposition (DED). PBF is the most widely adopted metal 3D printing technique for both laser and electron beam heating, the former being the most common approach.[36] Metal powder from a dispenser is spread in a thin layer of thickness $\sim$20–100 μm using a blade. The conductive heat flow for a laser or electron beam is related to thermal diffusivity D and specific heat per volume C_p.[37] Power density, Q, is given by the following:

$$\frac{Q}{C_p} = \frac{\partial T}{\partial t} - D\nabla^2 T$$

where $\frac{\partial T}{\partial t} = -v\frac{\partial T}{\partial t}$ = cooling rate, $Q = \frac{P}{2\pi r^2 \lambda}$, $T \sim \frac{Q(1-R)}{\rho C_p x}$ = temperature, P = power absorbed at the surface $\sim$100 kW/cm^2, r = beam spot radius, λ = absorption length, R = material

reflectivity, and ρ = material density. In DED, the thermal source—typically laser or electron beam—melts the powder or wire as it is being deposited on the substrate similar to an extrusion process and bears similarities to plasma arc-welding, in which a gas tungsten arc-based welding torch deposits metal from wire feedstock in an inert gas, which is milled to produce 3D structures.[38]

The commonest DED technique is powder-based laser deposition of metal[39]—the deposition head comprises laser optics, a pressurized powder nozzle, and inert gas tubing. The powder may be fluidized either by an inert gas or by ultrasonic vibration and focused into the laser at the substrate. The laser creates a melt pool ~0.25–1 mm diameter by 0.1–0.5 mm depth (*i.e.,* generating an average layer thickness ~0.25–0.5 mm) on the substrate.

Direct laser metal deposition involves feeding the metal powder into the inert gas jet ejected from a nozzle onto the laser-melt pool. The injected powder melts and solidifies as the laser moves rapidly to another position. The deposition head creates a track of solidified material as it scans, building a 3D part layer-by-layer. With layer thicknesses of 40 μm to 1 mm, build rates of 300 cm^3/h can be achieved. For complex structures, support material and/or a multiaxis deposition head are required. Three-axis systems are common, but 4- or 5-axis systems using rotary tables or manipulator arms are available.

DED techniques include laser-engineered net shaping (LENS), direct metal deposition, laser-based metal deposition, electron beam freeform fabrication (EBF3), and welding arc-based methods among others. They differ primarily in details of the thermal energy source and material delivery. LENS involves spraying metal powder (such as steel, Al, Cu, Ti, and even tungsten) into a metal melt pool created by Nd:YAG laser in a chamber with a controlled inert gas environment such as Ar.[40] Within the print head, the powder is supplied coaxially from a nozzle to the laser beam focused by a lens, where a metal melt pool is created. In fact, the metal particles do not become molten until they reach the melt pool. The powder most commonly uses gravity but can be conveyed by an inert gas such as He or Ar.

PBF technology using either a laser beam or electron beam heat source is the commonest of the metal additive manufacturing processes.[41] The beam interacts with metal powder by converting beam energy (hf for laser and $mv^2/2$ for electron) into thermal energy. PBF includes selective laser sintering/melting (SLS/M) and electron beam melting (EBM). The laser or electron beam energy source scans a pattern onto a bed of metal powder spread over the worktable. Where the powder is scanned, it forms a thin layer of sintered or melted metal, which then solidifies. Once each layer is complete, the work platform is depressed and another layer of metal powder is rolled across and the process repeated until the 3D part has been constructed. The powder bed may act as sacrificial support for overhanging features.

However, large overhangs may require tapering to reduce the need for dedicated sacrificial supports. Both DED and PBF approaches yield poor surface finish (~25 μm) and poor dimensional accuracy (~0.25 mm), with DED offering inferior small-scale featuring than PBF.

In SLS/M, a 200 W laser with a spot size of 500–100 μm is typically scanned using mirrors to melt the metal powder—part tolerance is limited to laser spot size, while the powder size determines layer thickness and surface smoothness. The 2-most commonly used lasers are CO_2 and Nd:YAG—the CO_2 laser operates at higher power and efficiency, but the higher frequency Nd:YAG laser exhibits higher absorptivity to the material and requires lower power. Absorptivity of most materials is much less at CO_2 laser wavelengths than at Nd:YAG laser wavelengths, and so, higher CO_2 laser power is required.

SLS/M involves using the laser to sinter or melt a layer of metal powder into a solid within a noble gas atmosphere—Ar for reactive metals or N_2 for nonreactive metals. The process is controlled through laser power, scanning speed, hatching distance, and layer thickness—the scan strategy requires the melt track to overlap the hatch distance. Hatching defines the spacing between the centers of 2 consecutive laser/electron beams and influences the trade of production speed, laser power, and material porosity. Selective laser melting (SLM) is an advanced form of SLS, which melts rather than sinters the powder to give denser parts. SLM has been used to fabricate pure tantalum to within >99% of full density.

However, SLS/M is not well suited to Al powders due to the formation of oxides on all its surfaces, which encourages balling.[42] Such oxide formation would not occur in the vacuum of the Moon. Fast cooling rates minimize nonequilibrium phases, secondary phases (such as carbide inclusions), and brittle intermetallic phases due to the fine structure imposed by rapid solidification. The rapid movement of lasers ensures high cooling rates ~10^3–10^5°C/s. Each thin layer fuses with the previously deposited layer as it is deposited by the laser beam that scans its 2-dimensional shape on the powder bed.

The Renishaw SLM facilities in Kitchener Ontario offer 200 and 400 W laser powder bed machines typically with a 70 μm laser spot size. The machines can be fitted with a reduced build volume to allow testing and parameter development on small quantities of powder. They can deposit a range of metallic alloys in powder form. *Figure 3* illustrates SLS-printed test structures from Ti powder created by the Metalysis FFC process.

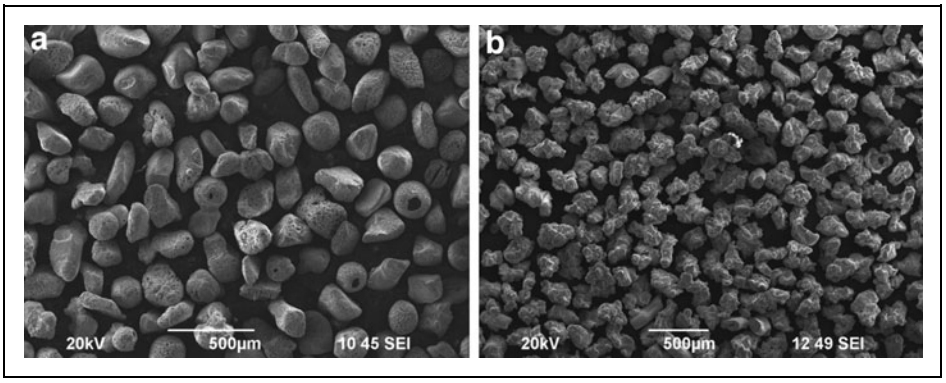

Fig. 3. (a) Synthetic rutile feedstock; (b) titanium powder resulting from reduced synthetic rutile powder.

SLS/M is a sophisticated 3D printing process suitable for different types of powdered material—metal, ceramic, glass, and polymer including tungsten as well as more commonly used metals.[43] Direct laser sintering of mixtures of elemental powders has yielded high-strength and hardness alloys.[44] Ceramics tend to crack due to the high temperatures required, which induce thermal shock on cooling—however, ceramic printing is feasible in a eutectic mixture to reduce the melting temperatures, for example, the introduction of Al_2O_3 to SiO_2 forms a salt eutectic mixture with a lower melting point that can be accommodated by solar concentrators.

Nevertheless, direct laser sintering of 50 µm ball-milled silica sand has been demonstrated using a 120 W CO_2 laser at 1,060 nm moving at 120 mm/s coupled with 400°C preheating of the powder bed sealed in nitrogen to yield localized 1,200°C melting and solidification in a spot size of 50–200 µm.[45] This technique may be exploited to build casting molds for metals. Selective laser sintering may also be used for polymers[46] although fused deposition modeling is far more common. Metal powder may be combined with a polymeric binder, which is deposited at low temperature. This is binder jetting uses 2 materials[47]—a metal/ceramic powder and a binder cementing the powder together.

The metal powder is spread and a layer of binder in liquid form is deposited over the powder layer. Each layer is deposited consecutively. Once the green part has been built, it can be bulk-sintered at high temperature—postcuring may also be necessary, which can be complicated, but it can process a wide range of materials; however, the part porosity is inferior to SLM and electron beam additive manufacturing (EBAM).

EBAM involves a high-power (around 4 kW), thermionically driven electron gun—a heated oxide-coated tungsten filament emits hot electrons that are accelerated at 60 kV to high velocity. They are focused into a beam spot of ~0.1 mm diameter by an electromagnetic lens formed by an electrical focusing coil and directed by a scanning magnetic field generated by a deflection coil. A metal powder is raked across the work platform into a 50–200 µm layer. The high-powered electron gun scans the metal particle bed where the electron kinetic energy is converted into thermal melting of the metal powder with a deposited power of $\sim 10^6$ W/mm^2 to generate 2,000°C peak temperatures followed by rapid cooling.

EBAM requires a vacuum of 10^{-4}–10^{-5} mbar, which reduces oxidation contamination and is sometimes supplemented by He gas to aid metal cooling. The process is controlled through multiple process parameters—beam power, scanning velocity, beam focus, beam diameter, line spacing, preheating strategy, platform temperature, and scanning strategy. Preheating the powder bed to bring the temperature close to the sinter temperature at 700–1,100°C reduces the energy requirements and reduces thermal stresses.

Deposited material is built up layer-by-layer to create fully dense 3D net shape parts with high strength without the need for further heat treatment. The material must have a low vapor pressure near its melting point, which includes most metals but excludes nonmetals as the electron beam needs to couple electrically to the material. Most metals—steel, nickel alloys, cobalt alloys, copper/nickel alloys, aluminum alloys, titanium alloys, tantalum and tungsten but not zinc, cadmium or magnesium alloys—can be electron beam processed. Electron beams are much more efficient in converting electrical energy into thermal energy than lasers; electron beams require a vacuum and powders are difficult to handle under microgravity conditions favoring wire feed (*Fig. 4*).

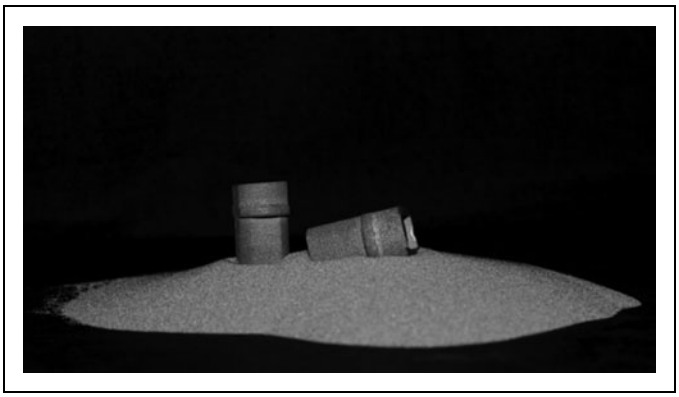

Fig. 4. 3D-printed structures from Metalysis FFC process-derived Ti powder.

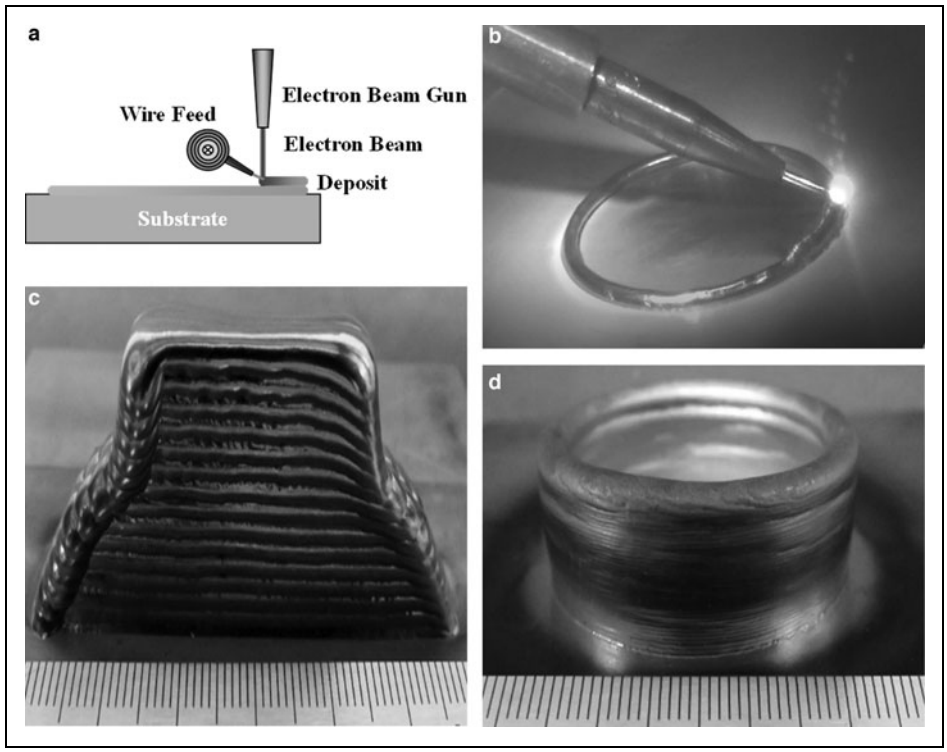

Fig. 5. Wire-fed EBAM **(a)** schematic of process, **(b)** Al alloy wire deposition, **(c)** Ti alloy structure, and **(d)** Ni alloy structure. EBAM, electron beam additive manufacturing.

EBM is similar to SLM except that an electron beam replaces the laser beam as the thermal source.[48] It operates similarly to a scanning electron microscope or electron beam welder. Electron beams have higher beam power but lower traverse speeds, yielding reduced cooling rates than lasers. To reduce layer corrugation, different layers may be deposited in randomly different scan directions. Wire feeding offers reduced porosity at the expense of dimensional accuracy. EBF3 is similar to direct laser deposition but based on electron beam welding.[49]

Metal wire feedstock—due to the difficulty in using powder in a vacuum—is melted in a 30–40 kW electron beam within a vacuum. It generates a focused electron beam in a high-vacuum chamber offering 100% feedstock consumption with 95% energy efficiency due to excellent electron coupling to the metal melt pool. The melted feedstock creates a molten pool only $\sim$10 μm thick on the substrate plate. EBF3 yields parts with excellent physical properties with high deposition rates of 2,500 cm^3/h.[50] EBF3 using wire feedstock is suited to rapid 3D printing of a wide range of metal alloys. Once the focused electron beam strikes the target, several types of emissions result requiring careful design and shielding: (1) low-energy secondary electrons $\sim$keV, (2) backscattered electrons; and (3) low-energy X-rays.

The National Research Council of Canada's Sciaky EBAM system is capable of depositing metallic materials in a vacuum operational environment using a wire feedstock (*Fig. 5a*, *b*). *Figure 5c* and *d* illustrates EBAM structures built from Ti alloy and Ni wires, respectively. Specific advantages of the EBAM process are the relatively large build envelope, near 100% material efficiency of the wire-feed into the melt pool and high bulk material deposition rates of 200–600 mm^3/s depending on feature size and material. Also, the build envelope of the EBAM, limited by the vacuum environment under terrestrial conditions, is not constrained on the Moon.

Microgravity testing of an EBAM system onboard NASA's reduced gravity aircraft demonstrated the deposition performance to be equivalent to 1 G conditions.[51] The sintered metal powder rods from the Metalysis FFC process may potentially be designed to be wire-fed into EBAM, but we are yet to demonstrate this.

The controlled processing parameters for SLS/M are laser power P $\sim$ 200 W, scan speed v $\sim$ 120 mm/s, hatch distance between tracks h $\sim$ 0.1 mm, and powder layer thickness d $\sim$ 20–100 μm, and for EBM are electron beam voltage (20–60 keV), current $\sim$1–50 mA, focus diameter $\sim$0.1 mm diameter, scan rate, preheat temperature, and powder layer thickness $\sim$50–200 μm. The delivered specific energy/area for full density in both cases is given by the following:

$$\varphi = \frac{P}{vhd} \sim 60 - 70 \text{ J/mm}^2$$

Electron beams offer higher build rates $\sim$80 cm^3/h compared with $\sim$5–20 cm^3/h for lasers due to the increased penetration depth and rapid scanning speed. Both SLM and EBAM can print common metals including stainless steel such as 316L, aluminum alloys such as AlSi10Mg, titanium alloys such as Ti6Al4V, nickel-based superalloys such as Inconel 625/718, and cobalt/cobalt-chromium superalloys such as CoCrMo. Volatile elements with relatively low boiling points such as Zn that generate turbulent melt pools are unsuited to additive manufacturing (Zn is rare on the Moon).

Similar arguments apply to Mg-based alloys, which we have discarded on the basis of their marginal utility on the Moon. Electron beams tend to yield rougher surface finish than lasers and inferior dimensional accuracy, but they yield stronger structures. Subsequent surface treatment may be implemented with electron beam glazing using a defocused beam. Electron beams are generally favored because electron beams are more efficiently generated than laser beams—electric power is a scarcer resource than thermal power on the Moon by virtue of electrical conversion losses.

Typically, postprocessing such as milling, polishing, shot peening, or hot isostatic processing (HIP) are commonly implemented—HIP is effective in removing surface porosity defects. In all additive manufacturing using thermal sources, high-energy deposition can cause residual stresses and layer warping. Residual stress occurs when melting a new layer on an underlying solid layer—as the molten layer solidifies, it contracts inducing shear stresses between layers, which can generate distortion of the part.

Preheating the build platform chamber to intermediate temperatures at ~200–500°C between the sample recrystallization and melting temperature and shorter scan lengths alleviates these high thermal gradients and the consequent internal stresses. Typically, the powder bed is subjected to a multipass, rapid preheating scan ~10 m/s to 40%–60% of melting temperature (nominally ~700–900°C) to reduce thermal gradients and so residual stresses.

This is followed by the melting stage at low scan speed ~0.5 m/s to melt the powder. The addition of postheating of layers can encourage annealing of thermal dislocation defects. Laser cusing divides each layer into a number of regions (islands) randomly selected for processing to reduce systematic stresses in the material.

The complex thermal cycling of rapid melting and then rapid solidification leads to high-temperature gradients and metastable microstructures. These high thermal gradients between layers can degrade the material's microstructure. Control of process parameters such as scan/print speed and thermal power to control the microstructure has proven difficult—lower scan speeds impart greater thermal power to the metal. However, the addition of nanoparticle inoculants mixed into molten metal can seed crystal nuclei during solidification, for example, ferrosilicon in iron[52] or hydrogen-stabilized zirconium in aluminum alloy.[53]

Although ferrosilicon is feasible, zirconium is not recovered in the lunar industrial ecology. Additive manufacturing is a relatively young technology that is continually improving with time, but it offers multiple advantages. It constitutes a single-technology system that is universal in its functional versatility to print sophisticated parts—including potentially electric motors constituting the key to printing entire robotic machines[54]—and is sustainable because of its uniqueness to minimize material waste and wasted energy on processing such waste.

CONCLUSIONS

We have examined the merits of the electrochemical Metalysis FFC process and its utility for lunar use. In particular, we took note of its low electrical energy consumption compared with its more readily available thermal energy consumption and the high purity of its metal output. We described 2 strategies for deploying the Metalysis FFC process: (1) for direct mineral reduction to produce mongrel alloys; and (2) with preprocessing before the process.

The need for a multitude of specific elemental metals for specific purposes suggests that the Metalysis FFC process may be supplemented with a modest set of geochemical preprocessing techniques. This provides the backbone of our lunar industrial ecology, a small network system of chemical processes in which there is minimal waste through recycling.

We then explored how the unique solid-state metal powders involved in the Metalysis FFC process lend themselves to the next stage of processing of metals using additive manufacturing, an approach that minimizes waste. In particular, the Metalysis FFC process in conjunction with metal 3D printing as part of an efficient processing chain appears a promising technological pair with widespread applications in the lunar context, potentially fulfilling the manufacture of components and systems of robotic machines of production.

Essentially, the 2 processes—the Metalysis FFC process and metal 3D printing—form the backbone of a manufacturing system to convert comminuted/beneficiated raw metal material into final products. These 2 methods in partnership offer unprecedented capabilities in deep ISRU of *in situ* manufacturing of final components directly from lunar material. Such a capability could provide for the *in situ* construction of productive capacity on the Moon with enormous transformative implications for space exploration.

For the future, we propose that a small technological demonstrator of the preprocessing methods, the Metalysis FFC process and additive manufacturing facility, should be constructed in preparation for a flight technical demonstration on the Moon in a small scale.

ACKNOWLEDGMENT

The authors thank Metalysis Ltd for the assistance and support for this article. There were, however, no financial transactions associated with this article.

AUTHOR DISCLOSURE STATEMENT

No competing financial interests exist.

FUNDING INFORMATION

No funding was received for this article.

SUPPLEMENTARY MATERIALS

Supplementary Data S1

REFERENCES

1. Matthews A. Crystallisation of anatase and rutile from amorphous titanium dioxide under hydrothermal conditions. Am Mineral. 1976;61:419–24.
2. Yang F, Hlavacek V. Effective extraction of titanium from rutile by a low-temperature chloride process. AIChE J. 2000;46(2):355–60.
3. Hu D, Dolganov A, Ma M, Bhattacharya B, Bishop M, Chen G. Development of the Fray-Farthing-Chen Cambridge process: Towards the sustainable production of titanium and its alloys. J Met. 2018;70(2):129–37.
4. Chen G, Fray D, Farthing T. Direct electrochemical reduction of titanium dioxide to titanium in molten calcium chloride. Nature. 2000;407:361–63.
5. Mohandas K, Fray D. FFC Cambridge process and removal of oxygen from metal-oxygen systems by molten salt electrolysis: An overview. Trans Indian Inst Met. 2004;57(6):579–92.
6. Jaio S, Fray D. Development of an inert anode for electrowinning in calcium chloride-calcium oxide melts. Metall Mater Trans B. 2010;41(1):74–9.
7. Dey S, Dhal C. Catalytic conversion of carbon monoxide into carbon dioxide over spinel catalysts: An overview. Mater Sci Energy Technol. 2019;2:575–88.
8. Rabl A. Comparison of solar concentrators. Sol Energy. 1976;18(2–4):93–111.
9. Hedgepath J, Miller R. Structural concepts for large solar concentrators. NASA CR-4075. 1987. https://ntrs.nasa.gov/citations/19870012561 (Last Acceesed on December 10, 2021).
10. Nakaruma T, Smith B. Solar power system for lunar ISRU applications. 48th AIAA Aerospace Sciences Meeting including the New Horizons Forum and Aerospace Exposition, Orlando, FL, AIAA 2010–1162. AIAA Reprint. 2010.
11. Gryaznov G, Zhabotinskii E, Zrodnikov A, Nikolaev N, Ponamarev-Stepnoi N, Pupko V, Serbin V, Usov V. Thermoemission reactor-converters for nuclear power units in outer space. Atomnaya Energiya. 1998;66(6):374–77.
12. Gyftopoulos E and Hatsopoulos G. Thermionic nuclear reactors. Electr Eng. 1963;108–16.
13. Meir S, Stephanos C, Gebelle T, Mannhart J. Highly efficient thermoelectronic conversion of solar energy and heat into electric power. J Renewable Sustainable Energy. 2013;5:043127.
14. Trucci D, Bellucci A, Cappelli E, Calvani P, Orlando S, Sciti D, Yogev R, Kribus A. (2012) Thermionic emission: A different path to solar thermal electricity. In: Proceedings on SolarPaces, Marrakesh, Morocco.
15. Kribus A, Segev G. Solar energy conversion with photon-enhanced thermionic emission. J Opt. 2016;18:073001.
16. Schwede J, Bargstin I, Riley D, Hardin B, Rosenthal S, Sun Y, Schmitt F, Pianetta P, Howe R, Shen X-Z, Melosh N. Photon-enhanced thermionic emission for solar concentrator systems. Nat Mater. 2010;9:762–7.
17. Shinke R, Bansode R, Bhosale C, Rajpure K. Physical properties of haematite α-Fe_2O_3 thin films: Application to photoelectrochemical solar cells. J Semiconductors. 2011;32:(1):013001.
18. Criswell D, Curreri P. Photovoltaics using in-situ resource utilization for HEDS. In: Proceedings on 6th ASCE Specialty Conf on Engineering Construction and Operations in Albuquerque, NM Space, 40339(206)34. 1998
19. Frendlich A, Ignatiev A, Horton C, Duke M, Curreri P, Sibille L. Manufacture of solar cells on the Moon. In: IEEE Record 31st Photovoltaic Specialists Conference. Lake Buena Vista, FL, 2005;794–7.
20. Schwandt C, Hamilton J, Fray D, Crawford I. Production of oxygen and metal from lunar regolith. Planet Space Sci. 2012;74:49–56.
21. Lomax B, Conti M, Khan N, Bennett N, Ganin A, Symes M. Proving the viability of an electrochemical process for the simultaneous extraction of oxygen and production of metal alloys from lunar regolith. Planet Space Sci. 2020;180:104748.
22. Oosthuizen S. In search of low-cost titanium: The Fray Farthing Chen Cambridge process. J South Afr Inst Min Metall. 2011;111(3):199–2006.
23. Papike J, Taylor L, Simon S. Lunar minerals. In: Heiken G, Vaniman D, French B, Schmitt J (ed.). Lunar Sourcebook: A User's Guide to the Moon. 1991:121–81.
24. Balla K, Roberson L, O'Connor G, Trigwell S, Bose S, Bandyopadhyay A. First demonstration on direct laser fabrication of lunar regolith parts. Rapid Prototyping J. 2012;18(6):451–7.
25. Pak V, Kirov S, Nalivaiko A, Ozherelkov D, Gromov A. Obtaining alumina from kaolin clay via aluminium chloride. Materials (Basel). 2019;12(23):3938.
26. Landis G. Materials refining on the Moon. Acta Astronaut. 2007;60:906–15.
27. Sargent P, Derby B. Advanced alloys and metal/ceramic composites from lunar source materials. Acta Astronaut. 1982;9(9):593–5.
28. Nohira T, Yasuda K, Ito Y. Pinpoint and bulk electrochemical reduction of insulating silicon dioxide to silicon. Nat Mater. 2003;2:397–401.
29. Jacob K, Srikanth S. Physical chemistry of the reduction of calcium oxide with aluminium in vacuum. High Temp Mater Processes. 1990;9(2–4):77–92.
30. Fenn A, Cooley G, Fray D, Smith L. Exploiting the FFC Cambridge process. Adv Mater Processes. 2004;51–2.
31. Tripathy P, Fray D. On the preparation of TiAl alloy by direct reduction of the oxide mixtures in calcium chloride melt. Fray International Symposium. In: Gibson I, Rosen D, Stucker B (eds.). Idaho National Laboratory, Additive Manufacturing Technologies, New York, NY: Springer Publishers, INL/CON-10-20068. 2011. https://inldigitallibrary.inl.gov/sites/sti/sti/5394111.pdf (Last Accessed on December 10, 2021).
32. Şafak K, Adams G. Modeling and simulation of an artificial muscle and its application to biomimetic robot posture control. Robot Auton Syst. 2002;41:225–43.
33. Lynch B, Jiang X-X, Ellery A, Nitzsche F. Characterisation, modelling and control of NiTi shape memory alloy based on electrical resistance feedback. J Intell Mater Syst Struct. 2016. DOI: 10.1177/1045389X16633764
34. Pham D, Dimov S. Rapid prototyping and rapid tooling—the key enablers for rapid manufacturing. Proc Inst Mech Eng C J Mech Eng Sci. 2003;217:1–23.
35. Cesaretti G, Dini E, De Kestellier X, Clla V, Pambaguian L. Building components for an outpost on the lunar soil by means of a novel 3D printing technology. Acta Astronaut. 2014;93:430–50.
36. Herzog D, Seyda V, Wycusk E, Emmelmann C. Additive manufacturing of metals. Acta Mater. 2016;117:371–92.
37. Murr L. Metallurgy of additive manufacturing: Examples from electron beam melting. Addit Manuf. 2015;5:40–53.
38. Gibson I, Rosen D, Stucker B. Directed energy deposition processes. Addit Manuf Technol 2015;245–68.
39. Copley S, Martukanitz R. Frazier W, Rigdon M. Mechanical properties of parts formed by laser additive manufacturing. Adv Mater Process. 2011;169:26–9.
40. Griffith M, Keicher D, Atwood C, Romero J, Smugeresky J, Harwell L, Greene D. Free form fabrication of metallic components using laser engineered net shaping (LENS^{TM}). Proc Int Solid Freeform Fabrication Symp. 1996.
41. Bhavar V, Kattire P, Patil V, Khot S, Gujar K, Singh. Review on powder bed fusion technology of metal additive manufacturing. In: Proceeding of 4th International Conference & Expo Additive Manufacturing Technologies, Bangalore, India. 2014.
42. Olakanmi E, Cochrane R, Dalgarno K. Review on selective laser sintering/melting (SLS/SLM) of aluminium alloy powders: Processing, microstructure and properties. Prog Mater Sci. 2015;74:401–77.
43. Pham D, Dimov S, Lacan F. Selective laser sintering: Applications and technological capabilities. Proc Inst Mech Eng B. 1999;233:435–49.
44. Sinchi A, Petzoldt F, Pohl H. On the development of direct metal laser sintering for rapid tooling. J Mater Process Technol. 2003;141:319–28.
45. Tang Y, Fuh J, Loh H, Wong Y, Lu L. Direct laser sintering of a silica sand. Mater Des. 2003;24:623–9.
46. Bourell D, Watt T, Leigh D, Fulcher B. Performance limitations in polymer laser sintering. Physics Procedia. 2014;56:147–56.

47. Gokuldoss P, Kolla S, Eckert J. Additive manufacturing processes: Selective laser melting, electron beam melting and binder jetting—selection guidelines. Materials. 2017;10:672.
48. Gong X, Anderson T, Chou K. Review on powder-based electron beam additive manufacturing technology. Manuf Rev. 2014;1:2–12.
49. Taminger K, Hafley R. Electron beam freeform fabrication (EBF3) for cost-effective near-net shape manufacturing. NASA TM 2006-214284. 2006. https://core.ac.uk/download/pdf/10516644.pdf (Last accessed on December 10, 2021).
50. Taminger K, Hafley R. Electron beam freeform fabrication: A rapid metal deposition process. In: Proceedings of Society of Plastics Engineers 3rd Annual Automotive Composites Conference. Troy, MI, 2003.
51. Hafley R, Taminger K, Bird R. Electron beam freeform fabrication in the space environment. In: Proceedings of 45th AIAA Aerospace Sciences Meeting & Exhibit. Reno, NV, 2007;1154.
52. Todd I. No more tears for metal 3D printing. Nature. 2017;549:342–3.
53. Martin J, Yahata B, Hundley J, Mayer J, Schaedler T, Pollock T. 3D printing of high strength aluminium alloys. Nature. 2017;549:365–9.
54. Ellery A. Universal construction based on 3D printing electric motors. In: IEEE International Symposium on Robotics & Intelligent Sensors (IRIS), Ottawa, Canada, 2017:81–5.

Address correspondence to:
Alex Ellery
Mechanical and Aerospace Engineering Department
Carleton University
1125 Colonel by Drive
Ottawa K1S 5B6
Canada

E-mail: aellery@mae.carleton.ca